中國機械工程學刊第四十三卷第三期第 265~274 頁(民國一百一十一年)
Journal of the Chinese Society of Mechanical Engineers, Vol.43, No.3, pp.265~274 (2022)

Reliability Analysis and Evaluation of Wheel Axle for High-Speed Train Considering Interference Fit

Yu-Ru Zhang*, Xin-Tian Liu** and Shuang-Long Geng*

Keywords： Reliability analysis, High-speed train wheel axle, Combined sleeve model, Interference fit.

ABSTRACT

The wheel axle is an important related component between high-speed train body and track, and the reliability of the connection between wheel and axle is directly related to the safe operation of high-speed train. The radial displacement of wheel axle interference surface has a great impact on the changes of interference amount. In this paper, based on the speed changes under actual train running conditions, the high-speed train wheel axle structure is simplified into a high-speed rotating ring combined sleeve model. Considering the interference fit and centrifugal force, the elastic mechanics of interference surface is analyzed to obtain the radial displacement. The reliability analysis model of high-speed train wheel axle is established on the basis of the stress intensity theory for axle equivalent stress and the variation for interference amount in allowable range. And the safety interval of wheel axle interference amount is determined by analyzing and evaluating the reliability of high-speed trains wheel axle. It has great application for the safe and reliable design of wheel axle for high-speed train.

INTRODUCTION

As the key component of the high-speed train, the wheel axle has an important influence on the high-speed railway safety [Xie et al, 2018, Makino et al, 2011]. To ensure the safe operation of high-speed trains, it is necessary to analyze and evaluate the reliability of wheel axles [Malika et al, 2014, Liu et al, 2017, Mao et al, 2021]. In the design of the train wheel and axle [Jin et al, 2020, Truman et al, 2007, Jin et al, 2019]. Excessive interference could cause the contact stress to increase, accelerate the damage of the wheel axle, and result in a shorter service life of the axle. If the interference is too small, the centrifugal force generated on the wheel and axle would reduce the interference amount under the high-speed movement of the train. Resulting in the contact stress unable to meet the connection of the wheel and axle and causing safety accidents [Lewis et al, 2008]. Therefore, to ensure the safety of train, interference fit connection between wheel and axle is also an important consideration in train design. Interference amount is an important index for reliability analysis and evaluation of high-speed train wheel axles [Zhang et al, 2021, Zhu et al, 2018]. By studying the interference fit of the axle, the basis is provided for checking the strength of the parts and calculating the transmission capacity. In this paper, based on the radial displacement equation under centrifugal force, the interference fit of wheel and axle is studied.

The train wheel and the axle are mainly connected by interference fit [Tornincasa et al, 2017]. The interference fit mainly uses the difference in the size of wheel hole and axle to cause deformation on their surface [Aleksandrova et al, 2016, Song et al, 2020]. And the contact stress generated by deformation makes wheel and axle form a tight bond [Zou et al, 2020]. During the rotation of wheel, the friction force generated by interference fit of wheel axle is employed to realize torque transmission. Pressure press-fitting method and temperature difference assembly method are often employed in the process of wheel and axle press-fitting [McMillan et al, 2015]. Pressure mounting method is to force axle into wheel hole. And the temperature difference assembly method is to process the two parts at different temperatures according to the method of thermal expansion and contraction [Zhang et al, 2021]. After the temperature drops to room temperature, the wheel and the axle will automatically form a close fit. Press-fitting method is the most common press-fitting method. During press-fitting, it is necessary to ensure reliability of the

Paper Received August, 2021. Revised January, 2022. Accepted February, 2022. Author for Correspondence: Xin-Tian Liu.

* *Graduate Student, School of Mechanical and Automotive Engineering, Shanghai University of Engineering Science, Songjiang, Shanghai 201620, China.*

** *Associate Professor, School of Mechanical and Automotive Engineering, Shanghai University of Engineering Science, Songjiang, Shanghai 201620, China.*

connection and ensure that the compressive stress could not be too high [Benuzzi et al, 2004]. Therefore, appropriate press-fitting force is an important factor to ensure the safety of the axle. Regardless of whether it is a strong press-fitting method or a temperature-difference press-fitting method, the surface of axle and surface of wheel hole after press-fitting would be deformed, and contact stress caused by the deformation is a crucial factor to measure the safety and reliability of the axle interference connection [Sekkal et al, 2018, Zarandi et al, 2019].

In engineering, ring sleeve model is the basic theoretical model to study the axle hole structure [Sharma et al, 2013]. In practical engineering, the train axle shaft is also designed based on the sleeve model principle, so that train wheel axle structure is simplified to the basic structure of the ring sleeve [Afaq et al, 2020]. Considering the difference in train speed under actual working conditions, through the elasticity analysis at interference surface of wheel axle, the effect of equivalent stress and radial displacement on interference of the high-speed rotating wheel axle is studied [Qiu et al, 2017, Zhang et al, 2000]. The initial interference between wheel and axles is analyzed according to the dimensional tolerance between the axles in engineering manufacturing [Lin et al, 2019]. Based on the above factors, a comprehensive analysis is carried out to determine the safe and reliable interference interval of the train axle.

In the future, high-speed trains will speed up according to the needs of development and the improvement of technology [Wang et al, 2019, Cheng et al, 2020]. Based on the research of the maximum speed of 800 km / h, the reliability analysis and evaluation [Zhu et al, 2020, Zhang et al, 2021] results obtained are safe and reliable for the train axles with the speed less than 800 km / h. This research has certain practical significance for the future speed increase of high-speed trains.

STRUCTURE OF TRAIN WHEEL AXLE

Wheel axle is an important structure to ensure the safe operation of the train. It is generally divided into trailer and EMU axle according to the types of train. As an important bearing part of the train, the reliability of the wheel axle is directly related to the safety of the train operation. The analysis of the safety and reliability of the wheel and axle has become an important part of the train design. In the design of train wheel axle, interference fit is generally used for the connection between wheel and axle. In order to meet the lightweight requirements of the train, the hollow axle structure is generally used. The hollow axle can not only reduce the weight of the train axle, but also provide enough strength to ensure the safety of wheel set. The train and axle are assembled in the train as a wheel set structure, which is shown in Figure 1.

The axle is only under the pressure of inner wall for wheel hub, the inner wall of wheel hub is only subjected to the pressure of axle. Therefore, the problem of wheel axle fit could be transformed into a combined cylinder model, which is analyzed according to the strength problem of thin-walled cylinder. The interference fit model of train axle structure is designed based on the principle of interference fit model of basic structure of combined ring sleeve, so it is simplified as interference fit model of basic combined ring sleeve structure.

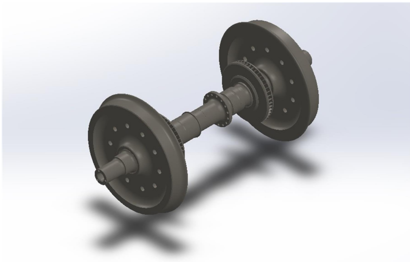

Fig. 1. Train wheel set structure.

INTERFERENCE FIT OF HIGH-SPEED TRAIN WHEEL AXLE

In the interference fit connection, the interference area between the mating surfaces is shown in Figure 2. The contact stress in this area can be analyzed according to the strength problem of thick-walled cylinder under plane stress state. The axle is only under the pressure of the inner wall of the wheel hub, the inner wall of the wheel hub is only subjected to the pressure of the axle. Therefore, the problem of wheel shaft fit could be transformed into a combined cylinder model, which could be analyzed according to the strength problem of thick-walled cylinder. The corresponding relationship between the two structural components is shown in Table 1.

Table 1. Corresponding relationship of structural components.

Structure of train wheel axle	Ring combination sleeve
Wheel hub	Outer tube
Wheel axle	Inner tube

When the maximum stress between the interference fit surface of wheel and axle is less than the maximum stress that the part does not produce plastic deformation. There is no plastic deformation on the surface of axle and wheel hole, and the connecting contact surface is in the state of elastic deformation. The contact stress between the mating surfaces could be deduced through the elastic theory.

In the press fit process, the size of interference has a great impact on the connection state of axle and wheel. If the interference is too small, the wheel and

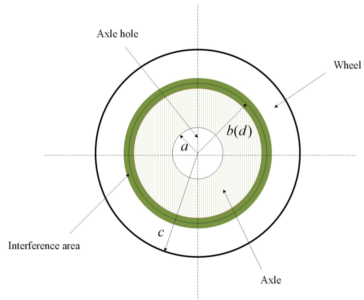

Fig. 2. Interference fit of train wheel axle.

axle slide relatively on the contact surface under the large torque, which lead to the reduction of power transmission efficiency and even the risk of wheel falling off. If the interference is too large, it is not only cause difficulty in pressing, but also cause axle damage in the process of pressing. The contact stress between wheel and axle exceeds the allowable range, which causes the wheel axle failure under the action of cyclic load, thus causing safety accidents. According to experience, the interference value between wheel and axle is controlled within 1.2-1.5‰ of wheel hub diameter.

Force analysis of ring model

The combined sleeve is composed of two ring models with interference, so the stress of ring should be analyzed first. Generally, the ring is subjected to internal and external pressure, which is shown in Figure 3(a). According to Lame formula [Vreede, 1992], under the action of internal pressure p_i and external pressure p_0, the stress at the position with radius r on the thick wall is denoted as:

$$\left.\begin{aligned}\sigma_\theta &= \frac{p_iR_i^2-p_0R_0^2}{R_0^2-R_i^2}+\frac{(p_i-p_0)R_i^2R_0^2}{R_0^2-R_i^2}\frac{1}{r^2}\\ \sigma_r &= \frac{p_iR_i^2-p_0R_0^2}{R_0^2-R_i^2}-\frac{(p_i-p_0)R_i^2R_0^2}{R_0^2-R_i^2}\frac{1}{r^2}\\ \sigma_z &= \frac{p_iR_i^2-p_0R_0^2}{R_0^2-R_i^2}\end{aligned}\right\} \tag{1}$$

where σ_θ is the circumferential stress on the cylinder, σ_r is the radial stress on the cylinder and σ_z is the longitudinal stress on the cylinder. R_0 and R_i are the inner diameter and outer diameter of the cylinder respectively.

Static analysis of combined sleeve model

Similar to the high-speed train axle, the two rings of combined sleeve model are connected by interference fit. After press fit in the manufacturing process, the structural interference fit is shown in Fig. 3(b).

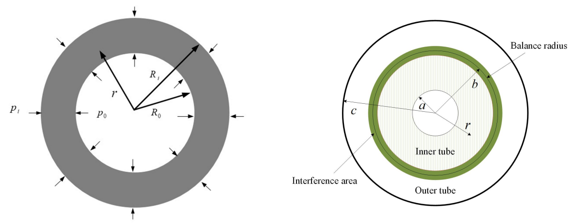

(a) (b)

Figure 3. (a) Stress condition of ring model, (b) Interference fit of ring combined sleeve.

According to the static equations, geometric equations and physical equations of the elasticity plane problem, the contact stress p_c of contact surface between two bodies in an interference fit is expressed as:

$$p_c=\frac{\delta}{2b}\frac{1}{\dfrac{c^2+b^2}{E_1(c^2-b^2)}+\dfrac{b^2+a^2}{E_2(b^2-a^2)}+\dfrac{\mu_1}{E_1}-\dfrac{\mu_2}{E_2}} \tag{2}$$

where E_1 and E_2 are the elastic modulus of the inner and outer sleeves respectively, δ is the interference amount. a is the inner diameter of the inner cylinder, b is the outer diameter of the inner cylinder, and c is the outer diameter of the outer cylinder.

According to the Lame formula [Vreede, 1992], the radial stress σ_{rci} and circumferential stress $\sigma_{\theta ci}$ generated by the interference fit on the hollow inner sleeve at any point with radius r are obtained by:

$$\sigma_{rci}=\frac{b^2p_c}{b^2-a^2}\left(\frac{a^2}{r^2}-1\right) \tag{3}$$

$$\sigma_{\theta ci}=\frac{-b^2p_c}{b^2-a^2}\left(1+\frac{a^2}{r^2}\right) \tag{4}$$

The radial stress σ_{rce} and circumferential stress $\sigma_{\theta ce}$ generated by the interference fit on the outer sleeve at any point with radius r are obtained by:

$$\sigma_{rce}=\frac{b^2p_c}{c^2-b^2}\left(1-\frac{c^2}{r^2}\right) \tag{5}$$

$$\sigma_{\theta ce}=\frac{b^2p_c}{c^2-b^2}\left(\frac{c^2}{r^2}+1\right) \tag{6}$$

Dynamic analysis of combined sleeve model

For the combined cylinder model with interference fits, the radius of outer wall for inner cylinder is larger than that of the inner hole for outer cylinder, so the radius size would change after fitting to reach the balance radius of interference fit. Since the walls of two cylinders are in the compression state, the outer wall of inner cylinder and the inner hole wall of outer cylinder will deform, which may be that both walls are in elastic deformation state. It may be that the inner hole wall of outer cylinder is in the state of elastic deformation, and the outer wall of inner cylinder is in the state of plastic deformation. It may be that the outer wall of the inner cylinder is in the state of elastic deformation, while the inner wall of the outer cylinder is in the state of plastic deformation as well. The state of deformation depends on the amount of interference, material type and size. When the combined cylinder is in the rotating state, the displacement would occur in the radial direction under the action of centrifugation. The change of displacement leads to the change of process quantity, which will affect the change of contact stress for inner and outer cylinder and the change of above stress.

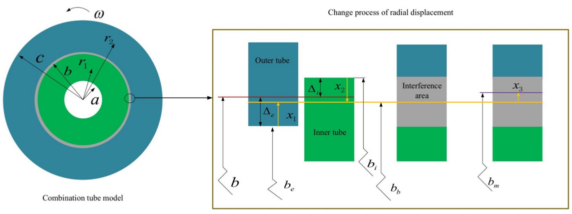

Figure 4. Interference fit analysis of dynamic combination sleeve.

In Fig. 4, b is the nominal radius of inner cylinder and outer cylinder, b_e is the actual radius of inner hole for outer cylinder, and b_i is the actual radius of outer ring for inner cylinder. b_b represents the contact boundary dimension of inner and outer cylinders after interference fit is balanced, b_m denotes the contact radius after the distance of equilibrium boundary movement under centrifugal force. Δ_e is the tolerance of inner hole radius dimension for outer cylinder and Δ_i is the tolerance of outer wall radius dimension for inner cylinder. x_1 represents the distance required to move the inner hole boundary when the inner hole of the outer cylinder reaches equilibrium boundary, x_2 denotes the distance that the outer wall radius of the inner cylinder needs to move to reach the equilibrium radius and x_3 is the distance of balance radius moving under the action of centrifugal force.

For the rotating composite tube structure, the elastic modulus of the inner tube and outer cylinder is E, Poisson's ratio is μ and the material density is ρ. When the inner and outer cylinders rotate at the same speed and the common angular velocity is ω, the centrifugal force is $\rho\omega^2 r$. A micro element is taken from combined cylinder for analysis, and unit length of the micro element is taken in the axial direction. As shown in Figure 5, the size of micro element is dr in radial direction and $d\theta$ in circumferential direction, then the displacement in the axial direction is $rd\theta$. The basic equations of elasticity in axisymmetric form should be satisfied.

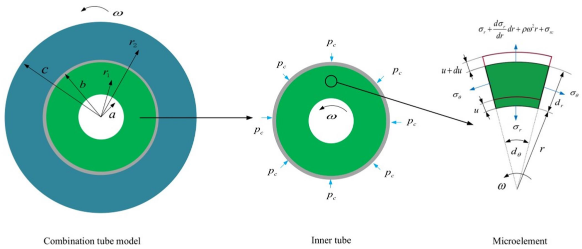

Fig. 5. Force analysis of dynamic combined sleeve.

Plane differential equation:

$$\left.\begin{aligned}&\frac{\partial\sigma_r}{\partial r}+\frac{\partial\tau_{rz}}{\partial z}+\frac{\sigma_r-\sigma_\theta}{r}=-\rho\omega^2 r\\&\frac{\partial\sigma_z}{\partial z}+\frac{\partial\tau_{rz}}{\partial r}+\frac{\tau_{rz}}{r}=0\end{aligned}\right\}\tag{7}$$

For the inner cylinder (round shaft):

Since it is simplified as a thin circular shaft, it can be expressed as a plane stress state, and the Equation 7 could be simplified as:

$$\frac{d\sigma_{ri}}{dr_1}+\frac{\sigma_{ri}-\sigma_{\theta i}}{r_1}+\rho\omega^2 r_1=0\tag{8}$$

Elastic constitutive equation of circular axis is shown as:

$$\left.\begin{aligned}&\varepsilon_{ri}=\frac{1-\mu^2}{E}\left(\sigma_{ri}-\frac{\mu}{1-\mu}\sigma_{\theta i}\right)\\&\varepsilon_{\theta i}=\frac{1-\mu^2}{E}\left(\sigma_{\theta i}-\frac{\mu}{1-\mu}\sigma_{ri}\right)\\&\sigma_{zi}=\mu\left(\sigma_{ri}+\sigma_{\theta i}\right)\end{aligned}\right\}\tag{9}$$

Geometric equation is expressed as:

$$\left.\begin{aligned}&\varepsilon_{ri}=\frac{(u_i+du_i)-u_i}{dr_1}=\frac{du_i}{dr_1}\\&\varepsilon_{\theta i}=\frac{(r_1+u_i)d\theta-rd\theta}{r_1 d\theta}=\frac{u_i}{r_1}\\&\gamma_{r\theta i}=\frac{dv_i}{dr_1}-\frac{v_i}{r_1}\end{aligned}\right\}\tag{10}$$

Subtracting the displacement u_i from the first two equations in the Equation (10), the strain coordination equation can be obtained as:

$$\varepsilon_{\theta_i}-\varepsilon_{r_i}+r_1\frac{d\varepsilon_{\theta i}}{dr_1}=0\tag{11}$$

Substituting the Equation (9) into the Equation (11) and defining the stress function φ_i, and $\varphi_i(r_1)=r_1\sigma_{ri}$, then:

$$\sigma_{\theta i}=\frac{d\varphi_i}{dr_1}+\rho\omega^2 r_1^2 \tag{12}$$

Eq. (11) is sorted as:

$$\frac{d^2\varphi_i}{dr_1^2}+\frac{1}{r_1}\frac{d\varphi_i}{dr_1}-\frac{\varphi_i}{r_1^2}+\left(3+\frac{\mu}{1-\mu}\right)\rho\omega^2 r_1=0 \tag{13}$$

Eq. (13) is integrated and φ_i is derived as:

$$\varphi_i=-\frac{3-2\mu}{8(1-\mu)}\rho\omega^2 r_1^2+C_1\frac{r_1}{2}+C_2\frac{1}{r_1} \tag{14}$$

where C_1 and C_2 are the integral constants.

Then, σ_{ri} and $\sigma_{\theta i}$ can be obtained respectively by:

$$\sigma_{ri}=\frac{\varphi_i(r_1)}{r_1}=-\frac{3-2\mu}{8(1-\mu)}\rho\omega^2 r_1+\frac{C_1}{2}+C_2\frac{1}{r_1^2} \tag{15}$$

$$\sigma_{\theta i}=\frac{d\varphi_i}{dr_1}+\rho\omega^2 r_1^2=-\frac{3\rho\omega^2 r_1^2}{8(1-\mu)}+\frac{C_1}{2}-\frac{C_2}{r_1^2} \tag{16}$$

According to the boundary conditions:

$$\left.\begin{aligned}\sigma_{ri}\,|_{r_1=a}&=0\\ \sigma_{ri}\,|_{r_1=b}&=-p_c\end{aligned}\right\} \tag{17}$$

C_1 and C_2 can be obtained as:

$$C_1=\frac{3-2\mu}{4(1-\mu)}\rho\omega^2\left(a^2+b^2\right)-2\frac{p_c b^2}{b^2-a^2} \tag{18}$$

$$C_2=-\frac{3-2\mu}{8(1-\mu)}\rho\omega^2 a^2 b^2-p_c\frac{a^2b^2}{b^2-a^2} \tag{19}$$

Substituting Eqs. (18) and (19) into Eqs. (15) and (16), σ_{ri} and $\sigma_{\theta i}$ could be obtained finally by:

$$\begin{aligned}\sigma_{ri}&=\frac{3-2\mu}{8(1-\mu)}\rho\omega^2\left(a^2+b^2-r_1^2-\frac{a^2b^2}{r_1^2}\right)\\ &\quad-\frac{p_c b^2}{b^2-a^2}-\frac{p_c a^2 b^2}{r_1\left(b^2-a^2\right)}\end{aligned} \tag{20}$$

$$\begin{aligned}\sigma_{\theta i}&=\frac{(3-2\mu)\rho\omega^2}{8(1-\mu)}\left(a^2+b^2+\frac{a^2b^2}{r_1^2}\right)\\ &\quad-\frac{1+2\mu}{8(1-\mu)}\rho\omega^2 r_1^2-\frac{p_c b^2}{b^2-a^2}+\frac{p_c a^2 b^2}{r_1^2\left(b^2-a^2\right)}\end{aligned} \tag{21}$$

Substituting the stress components into the Eq. (9) and Eq. (10), with the initial interference amount δ, the inner cylinder is at the radius r_1, and the radial displacement u_i can be expressed as:

$$\begin{aligned}&u_i(r_1)=\\ &\frac{\delta\rho\omega^2 r_1(3-2\mu)(1+\mu)(1-2\mu)\left(b^2+a^2\right)}{8E(1-\mu)\left(b^2-a^2\right)}\\ &\quad+\frac{\rho\omega^2 r_1^3(3-2\mu)(1+\mu)\left(2\mu^2-1\right)}{8E(1-\mu)(3-2\mu)}\\ &\quad+\frac{b^2a^2\delta\rho\omega^2 r_1(3-2\mu)(1+\mu)}{8Er_1^2(1-\mu)}\end{aligned} \tag{22}$$

For outer cylinder (disc):

Since it is simplified as a thin disk, it can be expressed as a plane stress state. Then the Eq. (7) could be simplified as:

$$\frac{d\sigma_{re}}{dr_2}+\frac{\sigma_{re}-\sigma_{\theta e}}{r_2}+\rho\omega^2 r_2=0 \tag{23}$$

The elastic constitutive equation of the disc is shown as:

$$\left.\begin{aligned}\varepsilon_{re}&=\frac{1}{E}(\sigma_{re}-\mu\sigma_{\theta e})\\ \varepsilon_{\theta e}&=\frac{1}{E}(\sigma_{\theta e}-\mu\sigma_{re})\\ \varepsilon_{ze}&=-\frac{\mu}{E}(\sigma_{re}+\sigma_{\theta e})\end{aligned}\right\} \tag{24}$$

Geometric equation is expressed as:

$$\left.\begin{aligned}\varepsilon_{re}&=\frac{(u_e+du_e)-u_e}{dr_2}=\frac{du_e}{dr_2}\\ \varepsilon_{\theta e}&=\frac{(r_2+u_e)d\theta-r_2 d\theta}{r_2 d\theta}=\frac{u_e}{r_2}\\ \gamma_{r\theta e}&=\frac{dv_e}{dr_2}-\frac{v_e}{r_2}\end{aligned}\right\} \tag{25}$$

Subtracting the displacement u_e from the first two equations in the Equation (25), the strain coordination equation can be obtained as:

$$\varepsilon_{\theta e}-\varepsilon_{re}+r_2\frac{d\varepsilon_{\theta e}}{dr_2}=0 \tag{26}$$

Substituting the Equation (24) into the Equation (26) and defining the stress function φ, and $\varphi(r)=r\sigma_r$, then:

$$\sigma_{\theta e}=\frac{d\varphi_e}{dr_2}+\rho\omega^2 r_2^2 \tag{27}$$

Eq. (26) is sorted as:

$$\frac{d^2\varphi_e}{dr_2^2}+\frac{1}{r_2}\frac{d\varphi_e}{dr_2}-\frac{\varphi_e}{r_2^2}+(3+\mu)\rho\omega^2 r_2=0 \tag{28}$$

Equation (28) is integrated and φ_e is derived as:

$$\varphi_e=-\frac{3+\mu}{8}\rho\omega^2 r_2^2+C_3\frac{r_2}{2}+C_4\frac{1}{r_2} \tag{29}$$

where C_3 and C_4 are the integral constants.

Then, σ_{re} and $\sigma_{\theta e}$ can be obtained respectively by:

$$\sigma_{re}=\frac{\varphi_e(r_2)}{r_2}=-\frac{3+\mu}{8}\rho\omega^2 r_2+\frac{C_3}{2}+C_4\frac{1}{r_2^2} \tag{30}$$

$$\begin{aligned}\sigma_{\theta e}&=\frac{d\varphi_e}{dr_2}+\rho\omega^2 r_2^2\\ &=-\frac{1+3\mu}{8}\rho\omega^2 r_2^2+\frac{C_3}{2}-\frac{C_4}{r_2^2}\end{aligned} \tag{31}$$

According to the boundary conditions:

$$\left.\begin{aligned}\sigma_{re}\big|_{r_2=b}&=-p_c\\ \sigma_{re}\big|_{r_2=c}&=0\end{aligned}\right\} \tag{32}$$

C_3 and C_4 can be obtained as:

$$C_3=\frac{3+\mu}{4}\rho\omega^2\left(b^2+c^2\right)+2\frac{p_c b^2}{c^2-b^2} \tag{33}$$

$$C_4=-\frac{3+\mu}{8}\rho\omega^2 b^2 c^2-p_c\frac{b^2c^2}{c^2-b^2} \tag{34}$$

Substituting Eqs. (33) and (34) into Eqs. (30) and (31), σ_{re} and $\sigma_{\theta e}$ could be obtained finally by:

$$\sigma_{re}=\frac{3+\mu}{8}\rho\omega^2\left(b^2+c^2-r_2^{\,2}-\frac{b^2c^2}{r_2^{\,2}}\right)+\frac{p_c b^2}{c^2-b^2}-\frac{p_c b^2 c^2}{r_2^{\,2}\left(c^2-b^2\right)} \tag{35}$$

$$\sigma_{\theta e}=\frac{\rho\omega^2 r_2^{\,2}(3+\mu)}{8}\left(b^2+c^2+\frac{b^2c^2}{r_2^{\,2}}\right)-\frac{\rho\omega^2 r_2^{\,4}(1+3\mu)}{8}+\frac{p_c b^2}{c^2-b^2}+\frac{p_c b^2c^2}{r_2^{\,2}\left(c^2-b^2\right)} \tag{36}$$

Substituting the stress components into the Eq. (24) and Eq. (25), with the initial interference amount δ, the inner cylinder is at the radius r_2, and the radial displacement u_e can be expressed as:

$$u_e(r_2)=\frac{\rho\omega^2 r_2\delta(3+\mu)(1+\mu)(1-2\mu)\left(c^2+b^2\right)}{8E\left(c^2-b^2\right)}+\frac{\rho\omega^2 r_2^{\,3}(3+\mu)(1+\mu)\left(2\mu^2-1\right)}{8E(3-2\mu)}+\frac{b^2c^2\rho\omega^2\delta(3+\mu)(1+\mu)}{8Er_2} \tag{37}$$

The interference amount δ_1 between the disc and the shaft under the action of centrifugal force is obtained by:

$$\delta_1=\delta-\left(u_e+u_i\right) \tag{38}$$

The equivalent stress σ_s is the main factor that affects the strength and life of the part. The equivalent stress of the surface of the axle and the inner wall of the hub is expressed as:

$$\sigma_s=\sqrt{\frac{1}{2}[(\sigma_1-\sigma_2)^2+(\sigma_2-\sigma_3)^2+(\sigma_3-\sigma_1)^2]} \tag{39}$$

where $\sigma_1=\sigma_\theta$, $\sigma_2=\tau_{r\theta}=0$, $\sigma_3=\sigma_r$.

Based on the above analysis of the interference fit of the circular ring combined sleeve, the analysis of interference fit for high-speed train wheel axle is consistent with it. It provides a theoretical basis for the following reliability analysis of high-speed train axles.

RELIABILITY ANALYSIS AND EVALUATION OF HIGH-SPEEDTRAIN WHEEL AXLE

Based on the stress intensity theory of equivalent stress and the change of wheel axle interference amount in allowable range, the reliability analysis model of high-speed train wheel axle is established. To analyze the influence of centrifugal force of high-speed train on the reliability of wheel axle, the force condition of train in static state is analyzed, and the position of maximum equivalent stress on wheel axle is determined. Then analyzing the changes of the interference for high-speed trains wheel axle under the influence of centrifugal force at different operating speeds, and the reasonable and safe interval of the high-speed train wheel axle interference amount is determined by analyzing the equivalent stress and the change of interference amount. The structure of train axle is shown in Fig. 6, and the axle parameters of high-speed train are shown in Table 2.

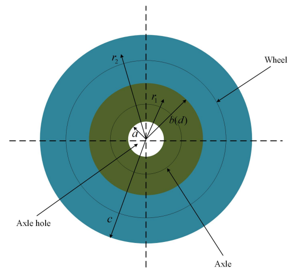

Figure 6. Structure of train wheel axle.

Table 2. Wheel axle parameters of high-speed train

Parameters	Symbol/unit	Value
Radius of axle hole	*a*/mm	65
Axis radius	*b*/mm	96
Wheel radius	*c*/mm	125
Wheel hole radius	*d*/mm	96
Elastic modulus	E/MPa	2.1×10^{11}
Poisson's ratio	/	0.3
Allowable stress of EMU axle	σ_1 / MPa	171
Allowable stress of trailer axle	σ_2 / MPa	200

In Fig. 6, r_1 and r_2 are the radii of calculation points on train axle and wheel respectively.

Allowable range of interference amount for wheel axle

Table 3 shows the dimension parameters of wheel hole diameter and shaft diameter. The nominal diameter of the shaft and the hole is 192mm, the lower deviation of the hole is -0.035mm, and the upper deviation is 0. According to the tolerance relation, it can be concluded that the wheel and shaft are in the state of interference fit. According to the interval calculation [Liu et al, 2018, Geng et al, 2019], the allowable range of interference amount for axle is obtained.

Table 3. Tolerance of Shaft and wheel and Interference

Assembly accessories	Diameter (mm)		Interference (mm)
	Hole	Axis	δ
Wheel	$\phi 192^{0}_{-0.045}$	$\phi 192^{+0.265}_{+0.185}$	[0.185, 0.3]

The tolerance range of the shaft Δ_a is shown as:

$$\Delta_a = [0.185, 0.265] \tag{40}$$

The tolerance range of the hole Δ_w is shown as:

$$\Delta_w = [-0.045, 0] \tag{41}$$

Then, the interference amount δ' is obtained as:

$$\delta' = \Delta_a - \Delta_w \tag{42}$$

According to the calculation, the allowable range of actual interference amount for axle is δ' = [0.185, 0.3]. The allowable range of interference is used to determine the safe and reliable range of interference.

Analysis of train wheel axle in static state

Based on the force analysis of the above combined sleeve, the initial interference is taken as 0.25mm, and the force of train wheel axle is analyzed in the static state.

As shown in Figure 7, the radial stress of axle increases with the increase of radius, the radial stress of axle is the largest at interference surface, and the circumferential stress of axle decreases with the increase of the radius. The radial stress of wheel decreases with the increase of the radius, the radial stress of wheel is the largest at interference surface, and the circumferential stress of wheel decreases with

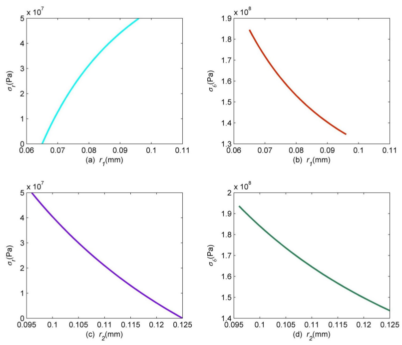

Fig. 7. Axle wheel stress without rotation.

the increase of radius. Based on above analysis, the maximum equivalent stress of axle appears at the interference fit contact surface for wheel and axle, so the equivalent stress at interference surface of wheel axle should satisfy strength requirements.

Analysis of the train wheel axle under high-speed rotation

Due to the high speed of the train, the components will move in the radial direction under the action of rotating centrifugal force. It is assumed that the part rotates around its axis at an equal angular speed, and the stress does not change along the axial direction, and the tangential rigid displacement component caused by rotation is not considered, only the relative deformation part is considered. Based on the dynamic radial displacement analysis theory of combined sleeve, the radial displacement and interference amount change of wheel axle at different speeds are analyzed, which is shown in Figure 8(a).

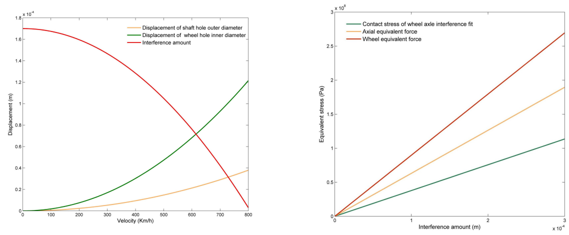

(a) (b)

Fig. 8. (a) Radial displacement and interference of wheel axle, (b) Equivalent stress of wheel axle.

In the case of high-speed driving, centrifugal force will be generated on the train wheels and axles, and the centrifugal force will change the interference between the wheels and axles. As shown in Fig. 8(a), under centrifugal action, as the vehicle speed continues to increase, the amount of deformation of the wheel holes and axles increases with the increase in vehicle speed. As the train speed increases, the interference amount between wheels and axles gradually decrease. In actual situations, when the friction provided by the interference cannot effectively satisfy the torque transmission between the wheel and the axle, the interference fit between the wheel and the axle will fail. The reduction in the amount of interference fit between the wheels and axles leads to a decrease in transmission efficiency and even the risk of wheels falling off, which seriously affects the safety of trains.

To further verify that the deformation of the high-speed train axle is elastic deformation, a reliability analysis model could be established based on the elastic deformation analysis of the above-mentioned combined sleeve, and the change analysis of the equivalent stress of the axle with the interference amount is shown in Fig. 8(b).

As shown in Fig. 8(b), the deformation of the wheel bore and the axle surface is within yield limit within the interference amount range of wheel axle. During the process of pressing the train wheel and axle, the surface of wheel hole and axle is still within the elastic deformation range. The press fit can be analyzed according to the elastic deformation. The reliability analysis and evaluation of high-speed train axle could be carried out based on elastic deformation theory.

RESULTS AND DISCUSSIONS

According to the radial displacement analysis of the train wheel axle under the centrifugal force, the actual size change of the wheel axle under the centrifugal force is obtained as shown in Figure 9(a).

In Fig. 9(a), the lower surface shows the actual size of wheel hole diameter changes with train speed and initial displacement. The upper surface shows the actual size of axle diameter changes with train speed and initial displacement. The intersection line of the curved surface is the position where the actual diameter of the axle and the actual diameter of the wheel hole are equal, that is, on this line, due to the centrifugal force, the interference amount of the wheel axle becomes 0. From the point of view of transmission torque and safety, the position before this intersection line is the safety limit of wheel axle interference fit. When the interference amount is reduced to a certain extent, not only can not the torque be transferred between the axles, but also the wheel will fall off. In the future, the high-speed train would speed up. Based on the centrifugal force, it is necessary to analyze the safety of the interference fit between the wheel and axle.

To comprehensively analyze the safe and reliable interference range of train axle under the action of centrifugal force, and comprehensively consider the influence of train speed and interference on the equivalent stress of axle, the overall analysis is carried out as shown in Fig. 9(b).

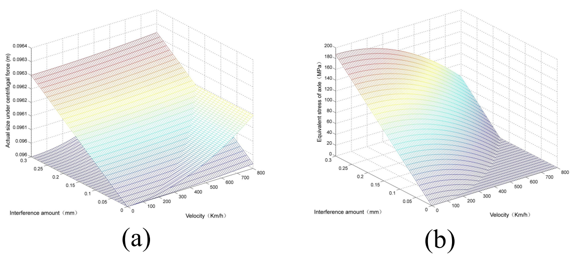

(a) (b)

Fig. 9. (a) Actual dimensions of wheel axle, (b) Equivalent stress of axle.

The allowable stresses on the axle positions of EMU axle and trailer axle are 170MPa and 200MPa respectively. At the wheel seat position, the stress of the motor car axle and trailer axle is 35.17MPa and 58.58MPa respectively. It can be seen from Fig. 12 that when the speed is 0 and the interference is 0.3mm, the equivalent stress on the axle surface is 187.6MPa. In addition, the stress generated by the external load on the wheel seat installation position has actually exceeded the allowable stress of the EMU axle and trailer axle. Under the interference of 0.3 mm, the fatigue strength of the wheel seat of the EMU axle is easy to be damaged. When the speed is 0 and the interference is 0.21mm, the equivalent stress on the shaft surface is 131.3Mpa, and the stress produced by the external load on the wheel seat installation position is within the allowable stress range. When the curved surface in the figure is at the curve at the junction of XY plane and curved surface, the equivalent stress of axle is 0, and the interference amount increases with the increase of train speed. This shows that the higher the speed is, the greater the interference is required when the equivalent force of train axle is 0, which is in line with the reality.

When the train runs normally, the speed is about 250km / h. When the train speed is 250km / h and the stress is equal to zero, the interference is about 0.01mm. When the interference is 0.17mm, the interference amount will become 0 when the train speed is greater than 800km / h. In order to ensure that the train axle can not only effectively transfer torque, but also not affect the fatigue life of the axle, the reasonable selection of interference amount is the key problem. According to the above analysis, it is safe that the interference is within 0.17-0.21mm, combining with the above allowable range, so the reasonable safe range of the train axle is 0.185-0.21mm.

Through the analysis of the safe range of interference when the train speed changes from 0 to 800 km / h, the wheel axle of high-speed train is also safe and reliable in this interference amount range when the maximum speed of the train reaches 800 km / h. According to the current speed of high-speed train, although it could not reach 800 km / h, in the near future, with the requirements of high-speed train technology and life, the train speed will certainly be greatly improved. The reliability analysis of high-speed train axle in this paper takes into account more than 2 times of the maximum speed of modern high-speed train, which has great application value for the safety and reliability of wheel axle under the condition of train speed increase in the future.

CONCLUSIONS

In this study, high-speed train wheel axle is simplified to a high-speed rotating combined sleeve. Reliability analysis model of the high-speed train wheel axle is established considering the interference fit and centrifugal force. The main conclusions are summarized as follows:

(1) The structure of train axle is simplified as a high-speed rotating ring combined sleeve model, and the change of interference amount of train axle under the action of centrifugal force and interference fit is considered. The reliability analysis model of wheel axle is established on the basis of the stress intensity

theory of axle equivalent stress and the variation of interference amount in allowable range.

(2) Through the elastic mechanics analysis of the interference fit of the train wheel axle, it is concluded that the deformation of the interference fit of the train axle under the normal operation condition is the elastic deformation. According to the elastic deformation, the influence of the equivalent force and radial displacement on the interference is analyzed. The safe range of interference is 0.185-0.21mm, which ensures that the train wheel axle could transfer torque effectively without fatigue fracture failure.

(3) Through the reliability evaluation, it is found that the interference amount obtained is safe and reliable when the speed of high-speed train is less than 800 km / h. It lays a theoretical and practical foundation for the future speed increase of high-speed trains.

REFERENCES

Afaq, A., Qaiser uz Zaman, K., and Ali, R., "Reliability analysis of strength models for CFRP-confined concrete cylinders," Compos. Struct., Vol. 244, pp. 112312 (2020).

Aleksandrova, Nelli., "Analytical Modeling in Deformation Analysis of Interference-Fit Structures," Structures, Vol. 6, pp. 30-36 (2016).

Benuzzi, D., and Donzella, G., "Prediction of the press-fit curve in the assembly of a railway axle and wheel," P. I. Mech. Eng. F-J. Rai., Vol. 218 No. 1, pp. 51-65 (2004).

Cheng, C., Wang, W.J., Luo, H., Zhang, B.C., Cheng, G.L., and Teng, W.X., "State-Degradation-Oriented Fault Diagnosis for High-Speed Train Running Gears System," Sensors, Vol. 20, No. 4, pp. 1017 (2020).

Geng, S.L., Liu, X.T., Liang, Z.Q., Wang, X.L., and Wang, Y.S., "Tolerance Analysis and Evaluation of Uncertain Automatic Battery Replacement System," Struct. Multidiscip. O., Vol. 61, No. 1, pp. 239-252 (2020).

Ishii, Kentaro., "Fatigue Strength and Maintenance of the Wheel-Axle Assembly for the Japanese Fast Train (Shinkansen)." J. Eng. Mater. Technol., Vol. 100, No. 3, pp. 227-232 (1978).

Jin, X.C., "A measurement and evaluation method for wheel-rail contact forces and axle stresses of high-speed train," Measurement, Vol. 149, pp. 106983 (2020).

Jin, X., "Evaluation and analysis approach of wheel–rail contact force measurements through a high-speed instrumented wheelset and related considerations," Vehicle Syst. Dyn., Vol. 58, No. 8, pp. 1189-1211 (2019).

Lewis, R., Yoxall, A., and Marshall, M.B., "Comparison of numerical and ultrasonic techniques for quantifying interference fit pressures." P. I. Mech. Eng. C-J. Mec., Vol. 222, No. 7, pp. 1125-1130 (2008).

Lin, B.L., Wu, J.P., Lin, R.X., Wang, J.X., Wang, H., and Zhang, X.H., "Optimization of high-level preventive maintenance scheduling for high-speed trains," Reliab. Eng. Syst. Safe., Vol. 183, pp. 261-275 (2019).

Liu, L., Liu, X.T., Wang, X.L., Wang, Y.S., and Li C.C., "Reliability analysis and evaluation of a brake system based on competing risks," J. Eng. Res.-Kuwait, Vol. 5, No. 3, pp. 150-161 (2017).

Liu, X.T., and Rao, S.S., "Vibration Analysis in the Presence of Uncertainties Using Universal Grey System Theory," J. Vib. Acoust., Vol. 140, No. 3, pp. 031009-031009-11 (2018).

Makino, T., Kato, T., and Hirakawa, K., "Review of the fatigue damage tolerance of high-speed railway axles in Japan," Eng. Fract. Mech., Vol. 78, No. 5, pp. 810-825 (2011).

Malika, M.S., Cavuto, A., Martarelli, M., Pandarese, G., and Revel, G.M., "Reliability Analysis of Laser Ultrasonics for Train Axle Diagnostics based on Model Assisted POD Curves," AIP Conference Proceedings, Vol. 1600, pp. 396-404 (2014).

Mao, K., Liu, X.T., Li, S.S., and Wang, X., "Reliability analysis for mechanical parts considering hidden cost via modified quality loss model," Qual. Reliab. Eng. Int., Vol. 37, No. 4, pp. 1373-1395 (2021).

McMillan, M.D., Booker, J.D., Smith, D.J., Fedorciuc, O.C., Korsunsky, A.M., Song, X., Baimpas, N., and Evans, A., "Analysis of increasing torque with recurrent slip in interference-fits," Eng. Fail. Anal. Vol. 62, pp. 58-74 (2015).

Qiu, J.X., Li, F.C., and Wang, J.F., "Damage detection for high-speed train axle based on the propagation characteristics of guided waves," Struct. Control. Hlth., Vol. 24, No. 3, pp. e1891 (2017).

Sekkal, W., Zaoui, A., Benzerzour, M., and Abriak, N., "Laser surface texturing of stainless steel 316L cylindrical pins for interference fit applications," J. Mater. Process. Tech., Vol. 252, pp. 58-68 (2018).

Sharma, S., and Yadav, S., "Thermo Elastic-Plastic Analysis of Rotating Functionally Graded Stainless Steel Composite Cylinder under Internal and External Pressure Using Finite Difference Method," Adv. Mater. Sci. Eng., No. 1–3, pp. 1-11 (2013).

Song, J.F., Song, Y.N., Wang, W.W., and Dong, Y.G., "Research on the Fretting Slip Characteristics of Interference Fit Surface of Train's Wheelset Running in Heavy Loads," J.

Physics Conference Series, Vol. 1637, pp. 012136 (2020).
Tornincasa, S., Bonisoli, E., Brino, M., "Tolerances and uncertainties effects on interference fit of automotive steel wheels," Lect. Notes Mech. Eng., pp. 665-674 (2017).
Truman, C.E., and Booker, J.D., "Analysis of a shrink-fit failure on a gear hub/shaft assembly," Eng. Fail. Anal., Vol. 14, No. 4, pp. 557-572 (2007).
Vreede, F.A., "Orthotropic Lame formulation of the constitutive equations for brittle rock," Mech. Mater., Vol.13, No. 3, pp. 193-205 (1992).
Wang, Z.W., Song, Y., Yin, Z.H., Wang, R.C., and Zhang, W.H., "Random Response Analysis of Axle-Box Bearing of a High-Speed Train Excited by Crosswinds and Track Irregularities," IEEE T. Veh. Technol., Vol. 68, No. 11, pp. 10607-10617 (2019).
Xie, G., Ye, M.Y., Hei, X.H., Qian, F.C., Cao, Y., and Cai, B.G., "Monitoring data-based aging analysis for the high speed train axle," IEEJ T. Electr. Electr., Vol. 13, No. 2, pp. 303-310 (2018).
Zarandi, Bagherinejad, S., Wei, H., and Wang, Y.C., "Sergey A. Residual Stress Analysis of an Orthotropic Composite Cylinder under Thermal Loading and Unloading," Symmetry, Vol. 11 No. 3, pp. 320 (2019).
Zhang, M.Y., Cai, Y.H., Chen, K., Mei, J., Yin, X.F., and Liu, J., "Research of Dynamic Stress on Assembly Process of Interference Fit Between Axle and Hole of Planetary Gear," Adv. Mater. Sci. Eng. III, Vol. 1247, pp. 210-219 (2021).
Zhang, Y.R., Liu, X.T., Lai, J.F., Wei, Y.W., and Luo, J., "Corrosion fatigue life prediction of crude oil storage tank via improved equivalent initial flaw size," Theor. Appl. Fract. Mec., Vol. 114, pp. 103023 (2021).
Zhang, Y.R., Liu, X.T., Yu, X.G., Wang, X., and Wang, X.L., "Reliability analysis of excavator boom considering mixed uncertain variables," Qual. Reliab. Eng. Int., Vol. 37, No. 4, pp. 1468-1483 (2021).
Zhang, Y., McClain, B., and Fang, X.D., "Design of interference fits via finite element method," Int. J. Mech. Sci., Vol. 42, No. 9, pp. 1835-1850 (2000).
Zhu, S.P., Keshtegar, B., Bagheri, M., Hao, P., and Trung, N.T., "Novel hybrid robust method for uncertain reliability analysis using finite conjugate map," Comput. Methods Appl. Mech. Engrg., Vol. 371, pp. 113309 (2020).
Zhu, S.P., Liu, Q., Peng, W.W., and Zhang, X.C., "Computational-experimental approaches for fatigue reliability assessment of turbine bladed disks," Int. J. Mec. Sci., Vol. 142, pp. 502-517 (2018).
Zou, L., Zeng, D.F., Wang, J., Lu, L., Li, Y., and Zhang, Y.B., "Effect of plastic deformation and fretting wear on the fretting fatigue of scaled railway axles," Int. J. Fatigue, Vol. 132, pp. 105371 (2020).

考慮過盈配合的高速列車輪軸可靠性分析與評估

張玉茹　劉新田　耿雙龍
上海工程技術大學機械與汽車工程學院

摘 要

輪軸是高速列車車體與軌道之間的重要關聯部件，輪與軸的連接可靠性也直接關係到高速列車的運行安全。輪軸過盈面的徑向位移對過盈量的變化影響很大。本文根據高速列車實際運行條件下的速度變化，將高速列車輪軸結構簡化為高速旋轉的圓環組合套筒模型。考慮過盈配合和離心力，對過盈面進行彈性力學分析，得到徑向位移。基於車軸等效應力的應力強度理論和過盈量在允許範圍內的變化，建立了高速列車輪軸的可靠性分析模型。通過對高速列車輪軸可靠性分析和評價，確定了輪軸過盈量的安全區間，對高速列車輪軸的安全可靠設計具有重要的應用價值。